Visual and functional demonstration of growing Bax-induced pores in mitochondrial outer membranes

Laura A Gillies[a], Han Du[b,*], Bjoern Peters[a], C. Michael Knudson[b], Donald D. Newmeyer[a,†], and Tomomi Kuwana[a,†]
[a]La Jolla Institute, La Jolla, CA 92037; [b]Department of Pathology, University of Iowa, Iowa City, IA 52242

ABSTRACT **Bax induces mitochondrial outer membrane permeabilization (MOMP), a critical step in apoptosis in which proteins are released into the cytoplasm. To resolve aspects of the mechanism, we used cryo-electron microscopy (cryo-EM) to visualize Bax-induced pores in purified mitochondrial outer membranes (MOMs). We observed solitary pores that exhibited negative curvature at their edges. Over time, the pores grew to ~100–160 nm in diameter after 60–90 min, with some pores measuring more than 300 nm. We confirmed these results using flow cytometry, which we used to monitor the release of fluorescent dextrans from isolated MOM vesicles. The dextran molecules were released gradually, in a manner constrained by pore size. However, the release rates were consistent over a range of dextran sizes (10–500 kDa). We concluded that the pores were not static but widened dramatically to release molecules of different sizes. Taken together, the data from cryo-EM and flow cytometry argue that Bax promotes MOMP by inducing the formation of large, growing pores through a mechanism involving membrane-curvature stress.**

Monitoring Editor
Carl-Henrik Heldin
Ludwig Institute for Cancer Research

Received: Nov 5, 2013
Revised: Oct 31, 2014
Accepted: Nov 12, 2014

INTRODUCTION

Apoptosis is a prominent type of active cell death in higher eukaryotes. The elimination of undesirable cells through apoptosis is important both for normal tissue homeostasis and for embryonic development and in diseases such as cancer (Hanahan and Weinberg, 2011). Clearly, therefore, understanding the molecular mechanism of apoptosis is relevant to human health. Most apoptotic signaling pathways converge on mitochondria to promote a critical event known as mitochondrial outer membrane permeabilization (MOMP). MOMP results in the release of proapoptotic proteins, such as cytochrome *c* and SMAC, that are normally confined to the mitochondrial intermembrane space (Liu *et al.*, 1996; Kluck *et al.*, 1997; Yang *et al.*, 1997). When released into the cytoplasm, these proteins trigger the activation of caspases, which cleave key protein substrates that carry out the apoptotic program. However, even if caspases are inactive for some reason, MOMP also initiates a progressive deterioration of mitochondrial composition and function, thereby incapacitating cells (Lartigue *et al.*, 2009). Thus MOMP is a critical event in apoptosis.

Apoptotic cell death is regulated by the Bcl-2 family of proteins, which function, in part, through a complex set of heterodimeric interactions localized in the mitochondrial outer membrane (MOM; Letai *et al.*, 2002; Chen *et al.*, 2005; Kuwana *et al.*, 2005; Chipuk *et al.*, 2010; Llambi *et al.*, 2011; Volkmann *et al.*, 2014). Bcl-2 family proteins belong to three functional subgroups that can be distinguished by how many of the Bcl-2 homology (BH) sequence domains, BH1–BH4, they possess. Two family members, Bax and Bak (containing BH1–BH3), are apoptotic effectors, which kill cells by promoting MOMP. Bax and Bak are constitutively present in cells but, under apoptotic conditions, are activated by certain Bcl-2 family members belonging to the BH3-only group (e.g., Bid, Bim, and Puma). On the other hand, the prosurvival members of the Bcl-2 family (e.g., Bcl-2, Bcl-xL, and Mcl-1) antagonize MOMP by

This article was published online ahead of print in MBoC in Press (http://www.molbiolcell.org/cgi/doi/10.1091/mbc.E13-11-0638) on November 19, 2014.

†These authors contributed equally to this work.

*Present address: College of Agronomy and Biotechnology, Southwest University, Chongqing 400715, China.

Address correspondence to: Tomomi Kuwana (tomomi@lji.org).

Abbreviations used: BH, Bcl-2 homology; cBid, cleaved Bid; cryo-EM, cryo-electron microscopy; DiI, 3H-indolium; 5-[[[4-(chloromethyl)benzoyl]amino]methyl]-2-[3-(1,3-dihydro-3,3-dimethyl-1-octadecyl-2H-indol-2-ylidene)-1-propenyl]-3,3-dimethyl-1-octadecyl, chloride; DLS, dynamic light scattering; F-dex, fluorescein-conjugated dextran; FITC, fluorescein isothiocyanate; MFI, median fluorescence intensity; MOM, mitochondrial outer membrane; MOMP, mitochondrial outer membrane permeabilization; OMVs, outer membrane vesicles.

heterodimerizing with Bax, Bak, and BH3-only proteins (Tanaka and Youle, 2008; Chipuk *et al.*, 2010).

Bax/Bak-induced membrane permeabilization has been analyzed both in whole cells and in cell-free membrane systems (Kluck *et al.*, 1997, 1999; Eskes *et al.*, 1998; Basanez *et al.*, 2002; Billen *et al.*, 2008). Recent molecular structure studies have elucidated some of the early conformational changes in Bax and Bak that accompany their activation (Dewson *et al.*, 2008; Dewson and Kluck, 2009; Gavathiotis *et al.*, 2008; Braun *et al.*, 2010; Czabotar *et al.*, 2013; Hilgendorf *et al.*, 2013; Moldoveanu *et al.*, 2013). However, the ultrastructural features of Bax/Bak-induced membrane permeabilization in the native MOM remain unexplored.

In our earlier work, we found that MOM vesicles (OMVs) loaded with very large fluorescent dextrans are capable of releasing those dextrans upon treatment with Bax and cBid (Kuwana *et al.*, 2002). We hypothesized that Bax-induced openings in the MOM, rather than being fixed-size proteinaceous pores, are large and form through a lipidic mechanism. To test this hypothesis, we used cryo-electron microscopy (cryo-EM) to visualize Bax-induced pores formed in native outer membranes. In parallel, we developed a functional assay to explore the manner in which Bax promotes macromolecular efflux through the MOM. Using flow cytometry, we followed the release of fluorescent dextrans from OMVs over time. On the basis of the concordance between our cryo-EM and flow-cytometry data, we gained insight into the mechanism through which Bax permeabilizes the MOM.

RESULTS

Direct visualization of Bax-induced outer membrane pores by cryo-EM

It is well established that activated Bax and Bak proteins permeabilize the MOM during apoptosis, causing the release of a number of proteins into the cytoplasm. The released proteins can be fairly large, for example, type-I RNA helicase (123 kDa; Van Loo *et al.*, 2002). However, investigations so far have failed to reveal details of the MOM structures that allow this macromolecular efflux. In particular, our earlier studies using thin-section and negative-stain electron microscopy (EM) were unable to detect any stable membrane alterations produced by Bax in the MOM (Kuwana *et al.*, 2002). In this study, we hypothesized that Bax permeabilizes membranes neither by disrupting them in a detergent-like manner nor by forming fixed-size proteinaceous channels. Rather, we predicted that Bax induces the formation of membrane pores that are supramolecular in scale, albeit fairly labile. To directly visualize Bax-induced membrane alterations, we used cryo-EM. This technique is challenging for structures as large as mitochondria but can capture transient and subtle membrane changes in a native, hydrated state.

In initial experiments, we were unable to preserve the structures of whole mitochondria in vitreous ice, perhaps because of the complexity and relative rigidity of these organelles. However, we succeeded in freezing isolated OMVs prepared from *Xenopus* egg mitochondria. Our previous work validated the use of OMVs to study the biochemical mechanisms of Bax-induced MOMP (Kuwana *et al.*, 2002; Kushnareva *et al.*, 2012). *Xenopus* egg OMVs are ellipsoidal and as large as isolated mitochondria (~600 nm by dynamic light scattering [DLS]; Supplemental Figure 2). Devoid of interior mitochondrial components, they consist only of resealed MOMs. Supplemental Figure 1 shows a low-magnification cryo-EM view. Because of their size, OMVs tended to reside in thick ice areas. In some areas of the grids, the OMVs displayed stretching artifacts that apparently arose from solvent flow during the freezing procedure. Therefore we carefully located regions in which multiple OMVs lacked such artifacts. In these areas, all the untreated OMV membranes were smooth and ellipsoid (Figure 1A). In contrast, when we incubated OMVs with Bax along with cleaved Bid (cBid, a BH3-only protein that activates Bax), many of the vesicles exhibited a single membrane pore. Often we observed areas of negative (i.e., inward or concave) membrane curvature flanking the pore (Figure 1B, asterisks). We note that these curvature effects are unlikely to result from sudden osmotic changes for two reasons: first, in these cryo-EM experiments, we did not load the OMVs with dextrans; second, MOMs are permeable to small molecules, as they contain VDAC (voltage-dependent anion channel) protein. Thus a significant osmotic pressure differential across the membrane cannot occur. Rather, the membrane curvature we observed is likely caused by the action of Bax in the membrane. The images strongly suggest that Bax-induced pores are formed by a lipidic mechanism that involves curvature stress.

By careful inspection of 1296 vesicles in undisturbed regions of the grid, we determined with a high degree of statistical significance that pores were present only in the Bax/cBid-treated OMVs (Figure 2A). Furthermore, as hypothesized, increasing the Bax concentration increased the frequency of OMVs with pores ($p = 0.0286$, one-tailed Mann-Whitney test). Importantly, the pores grew over time, reaching a mean diameter of ~60–90 nm after 20–30 min of incubation with Bax/cBid and ~100–160 nm after 60–90 min (Figure 2B). Also, the pores were wider when OMVs were incubated with a higher Bax concentration. Increasing the Bax concentration, however, did not cause more than one pore to form in each OMV. From this, we infer that integrated Bax molecules deform the membrane on a large scale but in a locally organized way. We saw no evidence of OMV doublets and therefore no sign of hemifusion, which had been proposed as a MOMP mechanism potentiated by Drp1 (Montessuit *et al.*, 2010). Indeed, our previous work showed that Bax-induced permeabilization of isolated rat and *Xenopus* OMVs does not involve Drp1 (Kushnareva *et al.*, 2012). Briefly stated, our OMV preparations do not contain detectable amounts of Drp1. Moreover, the addition of recombinant Drp-1 does not affect the release kinetics observed for rat or *Xenopus* OMVs, and OMV permeabilization is independent of GTP and ATP, which were previously shown to be required for the functions of Drp1. Paradoxically, mDivi-1 analogues (compounds that inhibit Dnm1, the yeast orthologue of Drp1) do inhibit Bax-induced permeabilization of rat (Kushnareva *et al.*, 2012) and *Xenopus* OMVs (unpublished observations). For the reasons just mentioned, these compounds apparently inhibit MOMP by targeting a still-unidentified MOM-resident protein distinct from Drp1.

A flow-cytometry assay to distinguish two modes of macromolecular release from native MOM vesicles: "gradual" and "all-or-none"

As a complement to this ultrastructural method, we developed a novel functional approach to follow the process of Bax-induced membrane permeabilization. Using flow cytometry, we analyzed the amount of fluorescein-labeled dextran (F-dex) contained within individual OMVs at various times after Bax activation. We predicted that, by examining the changes in the peak of fluorescent OMVs over time, we could distinguish between two possible modes of release: gradual and all-or-none (Figure 3A). The gradual mode of release would be manifested as a shift of the fluorescent vesicle peak to the left, that is, a reduction in median fluorescence intensity (MFI) corresponding to lower F-dex content. In contrast, the all-or-none mode would reduce the total number of vesicles that contained F-dex and simultaneously cause a low-MFI peak of empty OMVs to emerge.

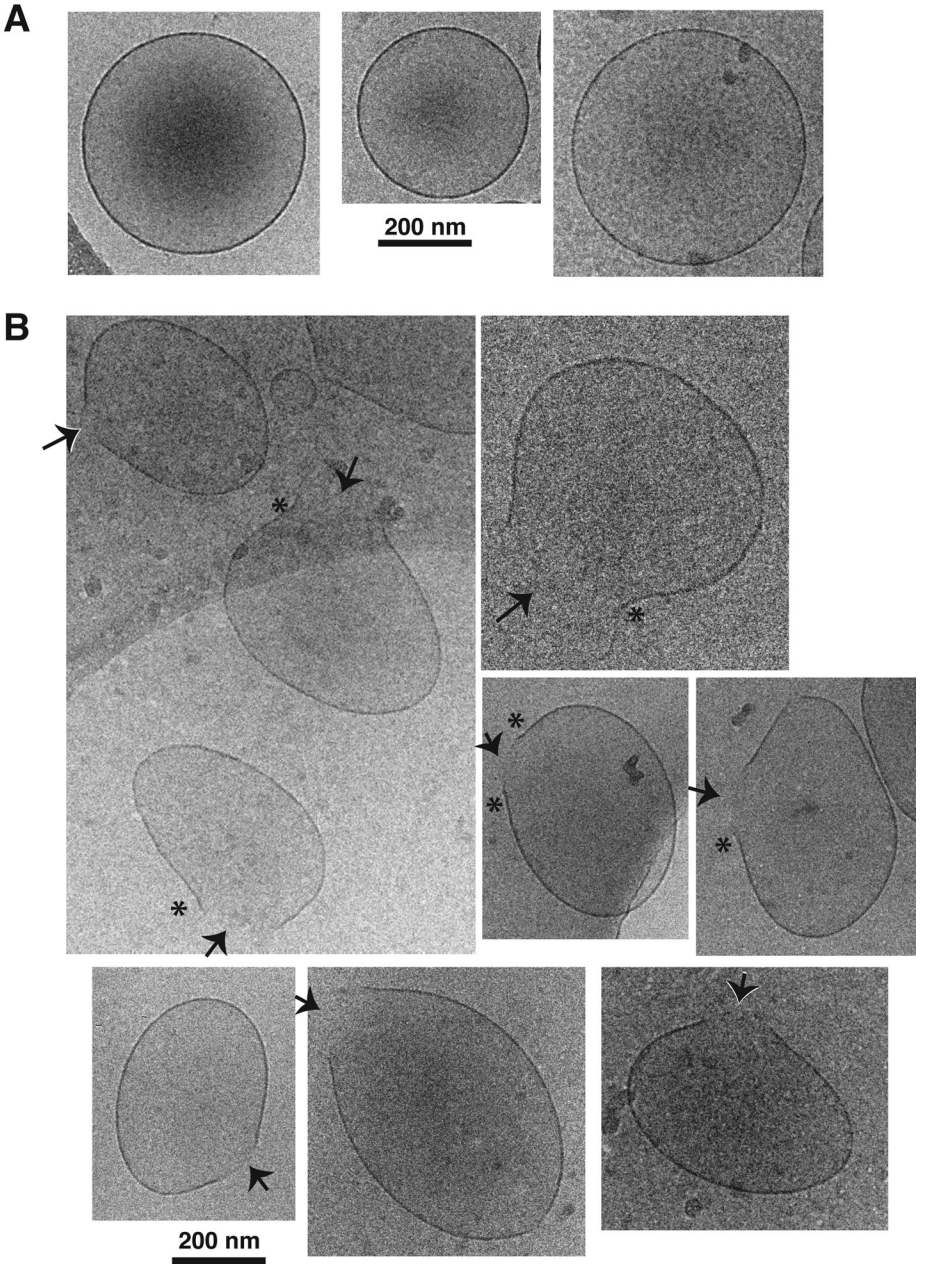

FIGURE 1: Cryo-EM imaging of OMVs permeabilized with Bax showing a solitary, large pore in many OMVs. (A) Untreated OMVs show round or ellipsoidal shapes with smooth membranes. (B) OMVs treated with Bax and cBid show only one pore per vesicle (arrows). Regions with negative curvature (asterisks) were often observed near the edges of the pores. The black spots are debris.

To analyze a nearly constant sample volume, we used a fixed sampling time; the instrumental flow rate was fairly constant, as illustrated by the reproducibility of OMV peak sizes over multiple runs (e.g., Figure 4, 0 nM Bax, at top). To avoid an artifact known as "swarm detection" (van der Pol *et al.*, 2012), in which multiple objects are counted together as a single event, we used a low flow rate and low concentrations of the vesicles. We could recognize the presence or absence of this swarm effect by a simple control, included in each experiment, in which we mixed dextran-loaded ("full") OMVs with Bax-permeabilized ("empty") OMVs. (In this case, Bcl-xL was added to the empty OMVs to prevent permeabilization of the full OMVs.) Under conditions producing the swarm artifact, a single peak appeared with an MFI intermediate between the full and empty OMVs (Supplemental Figure 3); this revealed that the instrument had registered the sum fluorescence intensities of OMV clusters rather than individual OMVs. On the other hand, under conditions in which the swarm artifact was avoided, the mixture of OMVs was resolved correctly into two well-separated peaks corresponding to the MFIs of the full and empty OMVs (e.g., Figures 3C and 4, bottom).

The OMV populations exhibited some size heterogeneity, as shown by side-scatter analysis. In two-dimensional plots of fluorescence versus side scatter (Supplemental Figure 4), the OMVs displayed a slanted distribution, showing that F-dex loading was essentially proportional to side scatter. When histograms of the fluorescence intensity were generated (projections on the fluorescence axis), this heterogeneity caused a considerable smearing of the OMV peaks. To better resolve the peaks, we devised a "slice" gate that restricted the analysis to a major subset of the population in the central portion of the side-scatter distribution (Supplemental Figure 4). This gating approach took advantage of our observation that the entire Bax-permeabilized OMV population shifted leftwards in this two-dimensional analysis; that is, the OMVs maintained a nearly identical side-scatter distribution throughout permeabilization (Supplemental Figure 4). Therefore, even though we ignored the tails of the distribution at high and low side scatter, we could be confident that the OMVs in the slice subset accurately represented the behavior of the whole population.

We further validated the flow-cytometry approach using simulation experiments done in the absence of added Bax. To mimic the gradual release mode, we loaded the vesicles with different concentrations of F-dex. As expected, reducing the internal concentrations of F-dex caused the peak to shift to lower fluorescence intensity (Figure 3B). We verified that these concentrations of F-dex loaded in OMVs did not produce fluorescence quenching (unpublished observations); therefore any decrease in MFI faithfully reflected the loss of F-dex from the vesicles. To simulate the all-or-none release mode, we mixed fully permeabilized and nonpermeabilized OMVs at set ratios. We observed the expected decrease and increase in the amplitude of the respective peaks (Figure 3C).

Additionally, we reasoned that we could probe the effective Bax-induced pore sizes by loading OMVs with F-dex of various molecular weights (10–500 kDa) under the assumption that the dextran molecules can only be released by pores of at least the same diameter. Published Stokes diameters for these dextran preparations were as follows: 10 kDa, 4.73 nm; 70 kDa, 11.6 nm; and 500 kDa, 29.4 nm

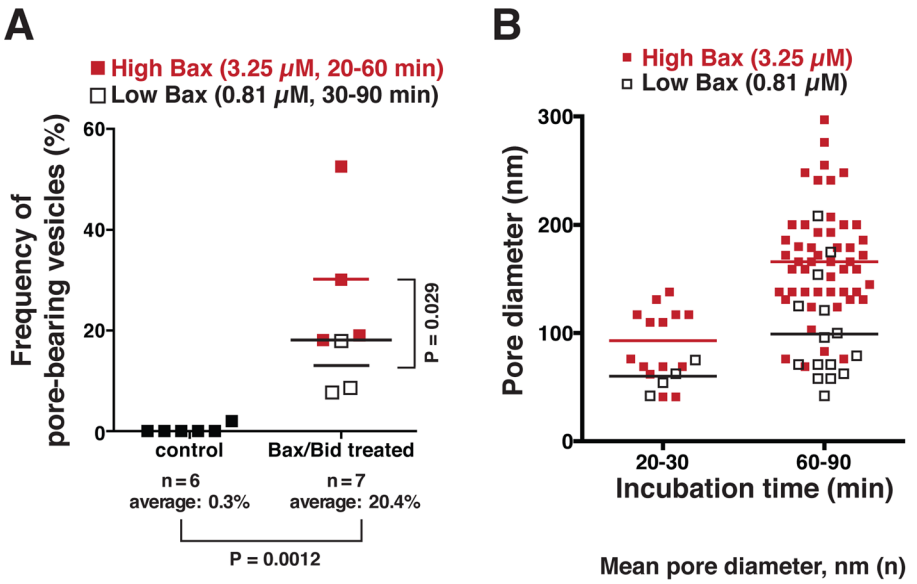

Mean pore diameter, nm (n)

	Early	Late
Low Bax	58 (4)	99 (15)
High Bax	91 (14)	159 (68)

Two way ANOVA

Interaction	P = 3.66
Bax	P = 0.003
Time	P = 0.0005

FIGURE 2: Bax-induced membrane pores increased in frequency and size with increased Bax concentration and incubation time. Untreated (663) and treated (633) vesicles were visualized by cryo-EM, counted, and categorized as pore-containing or smooth. (A) The frequency of pores in untreated OMVs was negligible, whereas this frequency ranged from 7.7% to 52.5% in Bax-treated OMVs. The difference was statistically highly significant (Mann-Whitney test: $p = 0.0012$), and thus pores were a feature only seen with Bax/Bid treatment. The frequency of OMVs containing pores was also higher with higher cBid/Bax input. (B) The pore size increased significantly with higher Bax concentration ($p = 0.003$) and with longer incubation time ($p = 0.0005$). "Low Bax" denotes the treatment with 812 nM Bax and 420 nM cBid; "High Bax" denotes treatment with 3.25 μM Bax and 2.5 μM cBid. Two-way analysis of variance showed there was no statistically significant synergy between time and Bax concentration.

(Granath, 1958). Using gel-filtration chromatography, we verified the molecular weights and Stokes diameters of the commercial dextran preparations (Supplemental Figure 5, A and B).

Bax forms large, growing pores in MOMs

After loading OMVs with F-dex, we incubated them with recombinant Bax, which was activated by the coaddition of recombinant cBid; we then obtained histograms of the F-dex content of OMVs at various times of incubation. We found that the entire OMV population underwent a gradual, progressive reduction in MFI, with only a minimal decrease in amplitude. We never observed a discrete peak corresponding to the MFI of empty OMVs, although at later time points we did see leftward tails on the main OMV peaks (Figures 4 and 5A). This suggested that activated Bax caused macromolecular release predominantly through the gradual mode. To confirm this more quantitatively, we analyzed the fluorescence histogram at each time point by curve fitting. Based on an inspection of the histograms, it was reasonable to assume that the OMV population was composed of some empty and some partly full OMVs. Accordingly, we fit the experimental histograms at each time point to the sum of two log-Gaussian distributions: one at a fixed MFI, corresponding to fully permeabilized OMVs (whose MFI we determined by incubating OMVs with a relatively high concentration of Bax for 2 h), and one with a variable MFI, corresponding to the peak of partially permeabilized OMVs. This is illustrated in Figure 5A.

Using the MFI and amplitude derived from these curve fits, we then calculated the contributions from the all-or-none versus the gradual release modes (see *Materials and Methods*; Figure 5B). We found that the contribution from the all-or-none mode of release was at most ~20%. This confirmed our conclusion that most of the F-dex molecules were released through the gradual mode. To measure the rates of gradual-mode dextran release, we fitted a simple exponential decay curve to the MFI values obtained at each time point (Figure 5C); as the number of intact OMVs was fairly constant, the rate of MFI change is essentially equal to the rate of gradual release (see *Materials and Methods*). In agreement with our previous experiments done on bulk populations of OMVs (Kushnareva *et al.*, 2012), we found that the rates of F-dex release showed an approximately linear dependence on Bax concentration (Figure 5D).

Surprisingly, however, the rates of dextran release were independent of dextran size (Figure 5D). It was paradoxical that both small and fairly large dextran molecules were released at nearly the same rates but, in all cases, mostly through the gradual mode, that is, through pores that limited dextran efflux. To resolve this conundrum, we were forced to conclude that Bax-induced pores grow gradually over time, reaching very large diameters. We reasoned that dextran molecules behave as slightly flexible random coils, and, although they are not rigid spheres, they diffuse very slowly through pores that are close in width to their Stokes diameter. As pores enlarge to widths greater than the Stokes diameter of the entrapped dextrans, the diffusion rate increases (Bohrer *et al.*, 1984). (An illustration of this hindered diffusion is provided by gel-filtration chromatography, in which macromolecules are retarded by passage through channels in the resin matrix.) Thus, at the moment the diameter of a Bax-induced pore widens sufficiently, the dextrans begin to escape gradually through the pore. Even though this pore-restricted efflux mode was slower than free diffusion, it was apparently rapid enough to allow ~80% of the dextran molecules to be released before the Bax-induced pore became substantially wider. Conceptually, once a membrane pore becomes much wider than the Stokes diameter of the entrapped dextrans, efflux of the remaining dextran molecules would become limited only by rates of free diffusion. In this situation, release would be essentially instantaneous on our experimental timescale. This is precisely the all-or-none mode of release. As our analysis shows, this type of sudden Bax-induced release could at most be accountable for 20% of the total. These results from flow cytometry, combined with our cryo-EM analysis above and DLS analysis (Supplemental Figure 2), allow us to conclude that Bax-induced MOMP does not produce a wholesale disruption of the

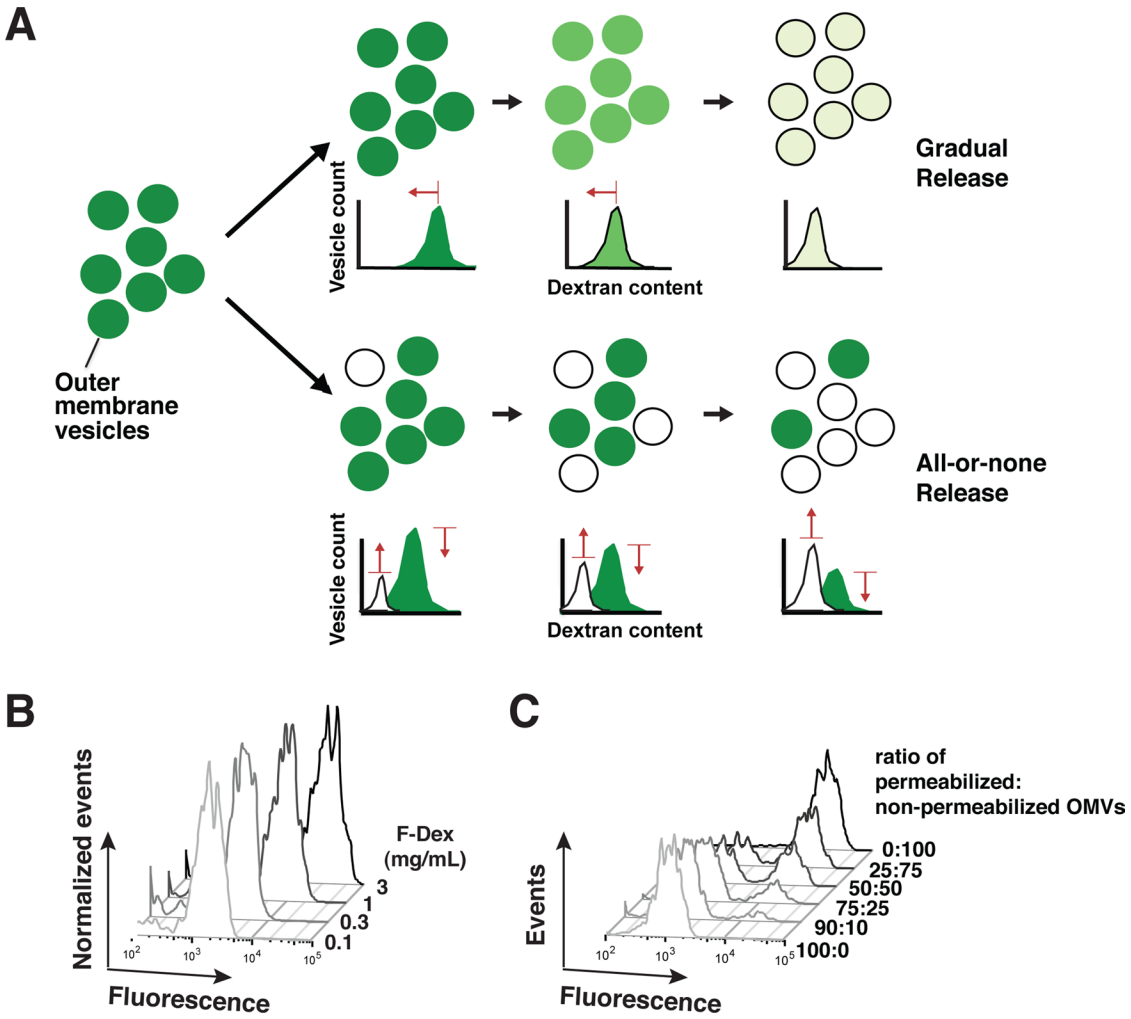

FIGURE 3: A flow-cytometry approach can analyze the fluorescence of individual OMVs and reveal trends in the overall population caused by Bax-induced MOMP. (A) Principle of the method. Over time, a leftward shift in the peak center (toward lower fluorescence intensity) would indicate gradual dextran release from the population of vesicles (top diagram). In contrast, a decline in the area under the peak (bottom diagram) would indicate that some of the vesicles had lost their entire content of fluorescent dextrans. At the same time, a low MFI peak corresponding to "empty" OMVs would emerge. (B) Experimental simulation of gradual release using OMVs loaded with varied amounts of F-dex. Reducing the dextran concentrations used for loading resulted in shifts of the OMV peak toward lower fluorescence intensity, as expected. (C) Experimental simulation of all-or-none release by dilution of the OMV suspension. This produced the predicted decline in amplitude of the full OMV peak and emergence of the empty OMV peak.

membrane but rather causes formation of pores that eventually grow to a diameter larger than the entrapped dextrans.

In summary, this flow-cytometry approach showed that Bax-induced pores grew slowly enough that most dextran molecules were released by a pore size–limited mechanism but rapidly enough that the release rates of different-sized dextrans were the same, at least up to 500 kDa (~30 nm in diameter). Cryo-EM produced comparable results, as it showed that Bax-induced pores grew to diameters of ~60–90 nm after 20–30 min.

DISCUSSION

Bax pores directly visualized in the native MOM are consistent with properties expected for MOMP in apoptosis

Activated Bax (or Bak) permeabilizes the MOM to release macromolecules from the mitochondrial intermembrane space during apoptosis. However, the precise nature of Bax-induced membrane alterations was unknown. To help clarify the mechanisms of Bax-induced outer membrane permeabilization, we imaged OMVs as they were undergoing permeabilization. We used cryo-EM, because this method can capture delicate ultrastructural changes in the hydrated state. In our experience, other traditional EM methods are unable to preserve Bax-induced membrane alterations (Kuwana *et al.*, 2002), likely because of artifacts introduced during sample preparation. For example, in negative-stain EM, a vesicle suspension is deposited onto the grid, and excess solution is aspirated. In the process, the vesicles become folded and flattened onto the grid surface and may dry out. Uranyl acetate stain is then added to the flattened structures. Clearly, vesicle morphology becomes distorted. In traditional thin-section EM, extensive dehydration, embedding, and staining steps contribute to the distortion or loss of delicate structural features. Thus it is not surprising that we and other investigators using these traditional EM techniques have failed to observe Bax-induced pores in whole isolated mitochondria and in mitochondria within apoptotic cells.

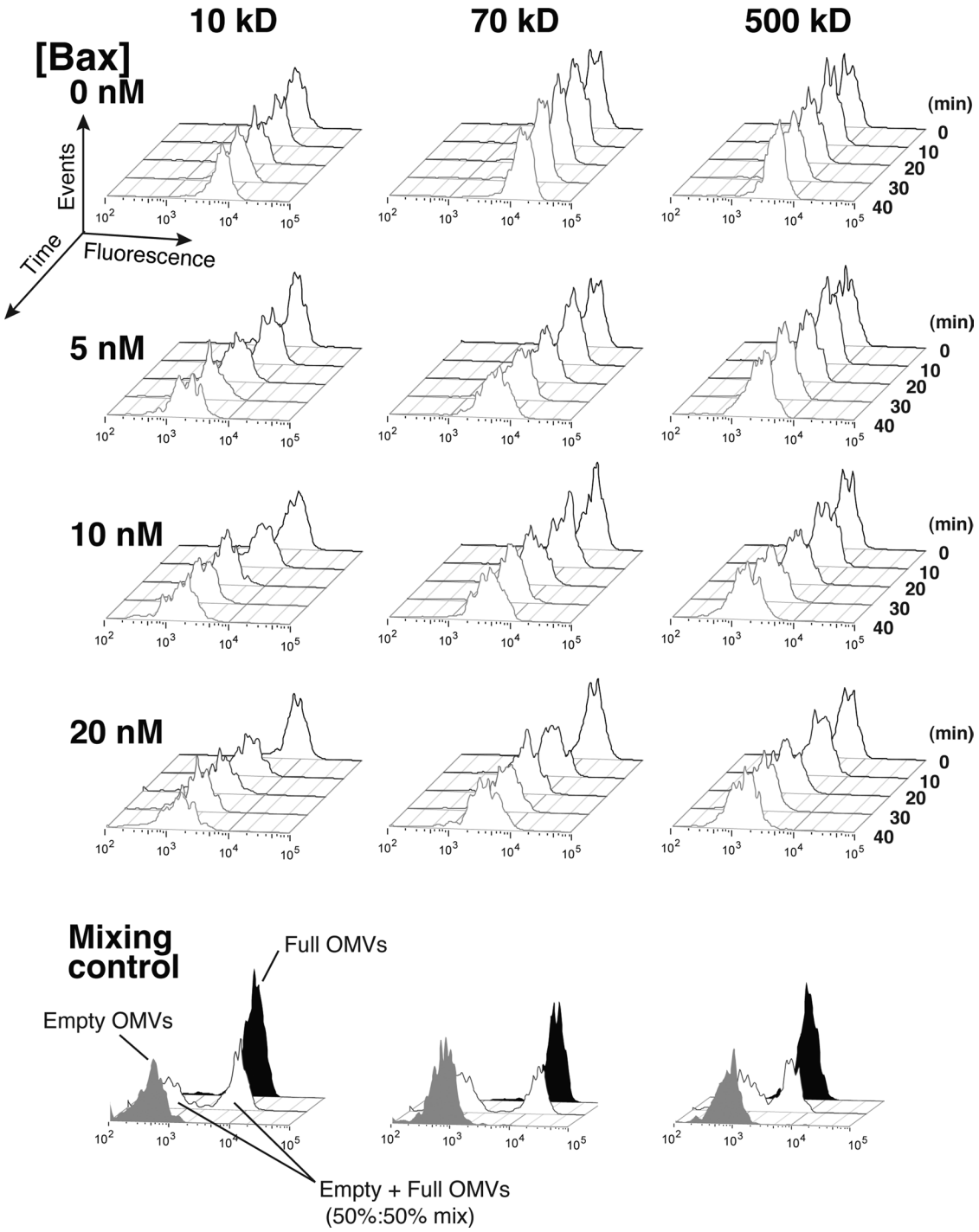

FIGURE 4: Bax-permeabilized OMVs shifted gradually toward lower MFI. OMVs loaded with 10-, 70-, or 500-kDa F-dex were treated with 0, 5, 10, or 20 nM Bax and 45 nM cBid and analyzed by flow cytometry every 5 min for 45 min. For clarity, histograms at every 10 min are shown. Data are representative of three independent experiments. Note that there were no discrete peaks at the MFI of the empty OMV peak (in solid gray) as shown in the control experiment for each dextran size (bottom panels). Rather, empty OMVs comprised only a tail to the left of the main peak; the main OMV peak gradually shifted toward lower MFI.

Unlike these traditional methods, cryo-EM clearly revealed that activated Bax formed pores in the MOMs that were typically larger than 60 nm (Figure 1B). The observed frequency of OMVs with visible pores (30% at the higher Bax concentration) may seem low, considering the near-complete dextran release we observed by biochemical assays. However, because OMVs are relatively large structures, it was necessary to use thick slabs of ice, which required the use of high-voltage instruments and resulted in images with very low contrast. Moreover, cryo-EM always shows structures in projection, and we therefore could only observe pores when their axes were perpendicular to the direction of the electron beam. As each OMV contained at most one pore, it is expected that many OMVs would appear to lack pores.

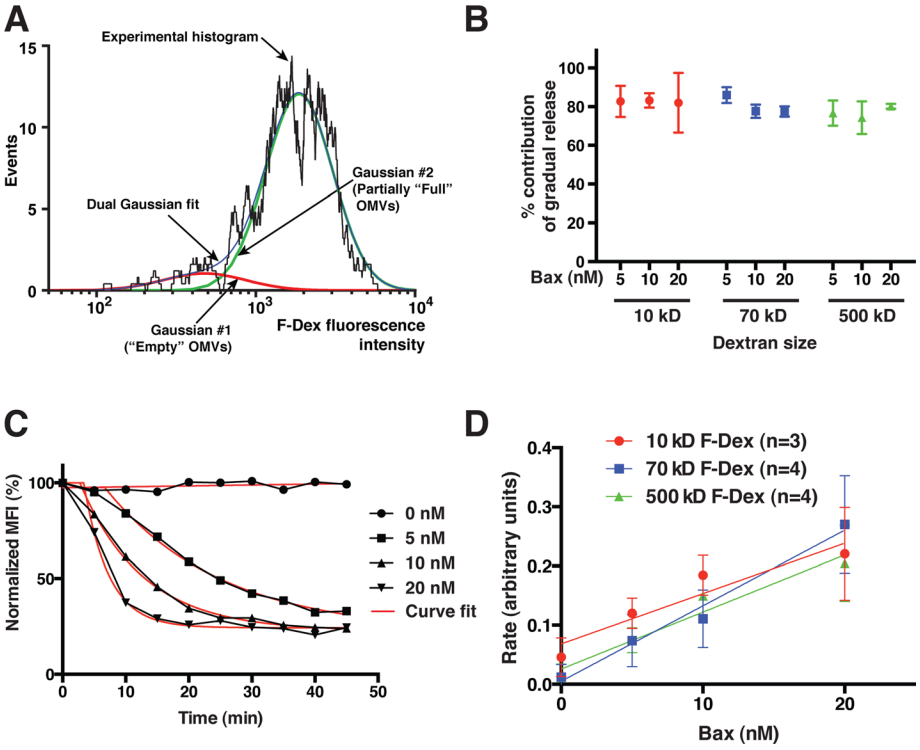

FIGURE 5: MOMP-associated F-dex release occurs predominantly by the gradual mode but is independent of dextran size. (A) An example of curve-fitting analysis from a 30-min time point. In this approach, we quantified the two forms of release as diagrammed in Figure 3. The MFI (peak center) of empty OMVs was estimated by treating OMVs with a relatively high concentration of Bax (20 nM) for 2 h. We then fitted the sum of two log-Gaussian peaks to the histograms at each time point, constraining one Gaussian curve to the MFI of the empty OMV peak and allowing a variable MFI for the second Gaussian curve representing the partially full OMV peak. Shown are the experimental histogram, the dual-Gaussian fitted curve, and the two component Gaussian distributions. Note that the empty OMVs comprise only a small tail on the left of the main peak and thus correspond to a much smaller Gaussian distribution. (B) Gradual release is predominant, regardless of dextran size and Bax concentration. Shown are the total contributions of gradual release for each dextran size at various Bax concentrations, calculated from the curve-fitting analyses described in *Materials and Methods*. Gradual release comprised ~80% of total release, independent of Bax concentrations or dextran size. (C) Example of a set of normalized MFI time courses fitted with simple exponential-decay curves. (D) Summary of the rates of change of MFI. These rates (which are essentially proportional to the rate of dextran release via the gradual mode) increased with Bax concentration and were similar for all F-dex sizes. Values show averages and SDs from three to four independent experiments.

sphingolipid metabolic enzymes (Chipuk *et al.*, 2012). Protein-free liposomes, which lack these factors, might not adequately reflect the physiological mechanism of pore formation.

However, we found here that pores induced by Bax in the native MOM closely resembled the structures we and others previously observed in liposomes incubated with activated Bax (Schafer *et al.*, 2009; Bleicken *et al.*, 2010; Landeta *et al.*, 2011). Therefore we propose that the basic pore-inducing function of Bax is the same for MOMs and liposomes. If so, then auxiliary proteins, such as the yet-unidentified catalyst (Kushnareva *et al.*, 2012), could act to enhance the intrinsic pore-forming activity of Bax and/or to promote the lateral mobility of Bax in the MOM.

In both liposomes (Schafer *et al.*, 2009) and OMVs (this study), we saw that the pore edges often exhibited negative curvature. Thus it is very likely that membrane curvature plays an important role in the formation of these apparently lipidic pore structures. Hints of this come also from earlier studies showing that incorporating membrane-curving lipids in liposome bilayers affects the ability of Bax to permeabilize the membranes (Basanez *et al.*, 2002; Montessuit *et al.*, 2010). Confusingly, however, these studies disagree as to whether lipids producing negative curvature promote or inhibit permeabilization. While it is still unclear exactly how curvature stress is involved, our work shows that Bax promotes negative curvature flanking the pores. This is consistent with an earlier report that very small liposomes are less responsive to Bax (Lucken-Ardjomande *et al.*, 2008), arguing that positive membrane curvature can inhibit Bax-induced membrane permeabilization.

An earlier study of liposomes permeabilized by Bax observed the transbilayer movement of a fluorescent dye, arguing that Bax forms pores that are not entirely proteinaceous (Terrones *et al.*, 2004). This behavior is reminiscent of the toroidal (lipidic) model postulated for pores formed by colicin or diphtheria toxin (Tilley and Saibil, 2006), molecules that have the same structural fold as Bcl-2 family proteins (Muchmore *et al.*, 1996). Although these studies with liposomes revealed an ability of activated Bax to form membrane pores, they left open the question of whether Bax permeabilizes native MOMs using the same lipidic mechanism. Indeed, our recent work highlighted two differences between liposomes and native MOMs: permeabilization of native MOMs is, first, kinetically more complex and efficient than that in liposomes; and second, involves a preliminary Bax-induced "catalyst activation" step, involving at least one resident MOM protein (Kushnareva *et al.*, 2012). Moreover, other studies have proposed that various proteins participate in MOMP, including Drp1 (Montessuit *et al.*, 2010), Bif-1 (Takahashi *et al.*, 2005; Etxebarria *et al.*, 2009), and

Solitary pores imply a large-scale organization of Bax in the membrane

Although it is well known that Bax spontaneously forms homo-oligomers in the MOM and in liposomes following activation, it still has not been formally proven that these oligomers are required for Bax-induced membrane pore formation. Indeed, recent studies using small nanodisk structures (Xu *et al.*, 2013) showed that a Bax monomer, when activated by a BH3-domain peptide, can integrate into the nanodisk lipid bilayer to form a 3.5-nm lipidic pore. This result is concordant with our recent studies showing that Bax monomers determine the kinetics of pore formation (Kushnareva *et al.*, 2012). A recent study measuring the membrane insertion of replacement cysteine residues in Bax concluded that helices α5 and α6 insert only shallowly in the lipid bilayer, suggesting a mechanism through which the insertion of Bax molecules could generate membrane-curvature stress (Westphal *et al.*, 2014).

It is still unclear how the smaller membrane deformations caused by Bax monomers lead to the solitary supramolecular-scale pores

observed here in OMVs. A commonly held hypothesis is that the pores are ringed by Bax oligomers that lengthen over time through autoactivation, thereby causing pore enlargement. Another possibility is that, during the initial stages of pore formation, the small Bax monomer–induced lipidic pores coalesce to form larger lipidic pores. To be able to observe these earlier states of pore enlargement would require a technological advancement, perhaps the cryo-EM imaging of gold-labeled Bax, or the analysis by cryo-EM averaging techniques of nanodisks that are able to accommodate more than one Bax molecule.

Nevertheless, it is significant that we observed only a single huge pore in each OMV and that increasing the Bax concentration produced a widening of this solitary pore. From this, we can deduce that the process through which Bax molecules contribute to pore enlargement is somehow organized around an existing membrane deformation. Otherwise, we would have observed multiple smaller pores. On the basis of our cryo-EM images, we propose that pore enlargement involves a feed-forward loop, that is, a concerted process. Integrated Bax monomers would promote membrane curvature, which in turn would favor the lateral migration of other Bax monomers to these areas of membrane curvature (Bax oligomerization could participate at this step), thus increasing the size of the membrane deformation. In time, curvature stress would build up until it finally overcomes the energy barrier for pore formation. Thereafter, the membrane curvature at the edges of the pore would continue to attract more Bax molecules, resulting in continuous pore enlargement.

Flow cytometry demonstrates growing pores induced by Bax in the MOM, consistent with cryo-EM data

Most previous assays of macromolecular release using single cells or bulk populations of mitochondria or OMVs were not intended for measuring the permeabilization of individual vesicles or organelles. For that purpose, we developed a flow-cytometry approach. The flow data showed that Bax-induced efflux of molecules through the MOM occurred predominantly by a pore-restricted mode ("gradual" release; Figure 3A). We interrogated pore sizes by comparing the release of different sizes of dextrans and saw no evidence of a sieve effect. That is, large dextrans were released at nearly the same rate as smaller dextrans; however, in each case, dextrans were released in a gradual manner, that is, via a pore-restricted mechanism. Somewhat conflicting results were recently reported in a study using giant unilamellar vesicles and fluorescence microscopy (Bleicken *et al.*, 2013). These authors observed the gradual release of a large polypeptide (104 kDa) but all-or-none release of cytochrome *c* (12 kDa). Also, they found that lower concentrations of Bax produced a greater contribution of gradual-mode release. These results may differ from ours due to their use of an artificial membrane system.

Previously, experiments utilizing patch-clamp analysis estimated that Bax-induced channels in the MOM grow only to 6 nm in diameter, at which point they stabilize (Guihard *et al.*, 2004; Dejean *et al.*, 2005; Martinez-Caballero *et al.*, 2009). The aforementioned study with giant unilamellar vesicles found that Bax-induced pores grow wider than this but still eventually reach a stable size or shrink (Bleicken *et al.*, 2013). Our data are inconsistent with these observations, as we saw no evidence that Bax-induced pores stabilized at any particular size. Remarkably, some of the pores grew to comprise a significant percentage of the diameter of the OMV itself (e.g., Figure 2B). Thus, in contrast to the conclusions of Bleicken and colleagues, our results argue that the curvature stress (which promotes pore enlargement) is generally always greater than the line tension at the OMV pore rim (which opposes pore enlargement). Our flow-cytometry data similarly imply that Bax-induced pores grew markedly, over the course of a few minutes or tens of minutes, with the rate of growth depending on Bax concentration. Thus our flow analysis confirmed that some Bax-induced pores grew to more than 30 nm in diameter within 45 min of incubation, essentially agreeing with our cryo-EM data.

The size-indiscriminate macromolecular efflux we observed here explains previous observations that proteins of different sizes are released from a single cell's mitochondrial population over the same short time period (Munoz-Pinedo *et al.*, 2006). As a corollary to this, we conclude that, in those cellular settings in which a differential release of certain mitochondrial proteins is observed (Munoz-Pinedo *et al.*, 2006; Estaquier and Arnoult, 2007), the explanation cannot involve the nature of Bax pores in the MOM. Rather, the difference likely arises because some proteins are soluble, while others must become detached from membranes to be released. In conclusion, our independent visual and functional approaches both show that activated Bax permeabilizes the mitochondrial membrane by promoting the formation of membrane pores that grow to be very large. The size and structure of these pores suggest that they are lipidic in nature and formed or enlarged by a mechanism involving curvature stress.

MATERIALS AND METHODS

OMVs from *Xenopus* egg mitochondria, recombinant full-length Bax, and cBid

These materials were generated with our published protocols (Kuwana *et al.*, 2002). We used the membrane-binding fluorescent dye, DiI (3H-indolium, 5-[[[4-(chloromethyl)benzoyl]amino]methyl]-2-[3-(1,3-dihydro-3,3-dimethyl-1-octadecyl-2H-indol-2-ylidene)-1-propenyl]-3,3-dimethyl-1-octadecyl, chloride; V-22888; Life Technologies, Carlsbad, CA) to label OMV membranes to assist with detection of these small particles by flow cytometry. Briefly, 300 µl of 0.1 mg/ml OMVs (as protein) was incubated with 2 nM DiI in 10 mM HEPES (pH 7.4) containing 1 mM EDTA for 45 min at room temperature. DiI-labeled OMVs were collected by centrifugation at 125,000 × *g* for 20 min at 4°C. The pellet was washed in the same buffer and collected again by centrifugation as above. Formerly, cBid was referred to as "N/C-Bid," meaning that, although the molecule is cleaved by an endoprotease, the N- and C-terminal portions remain associated.

Flow cytometry

Flow cytometry was performed on a BD Biosciences FACS Fortessa equipped with a high-throughput sampler for sample introduction from 96-well plates. Analysis was performed at a fixed volume of 30 µl of sample and a flow rate of 0.5 µl/s, resulting in a fixed sample-collection time of 1 min per well. All buffers utilized for the Fortessa were passed through a 100-nm filter before use. However, to further enhance collection of the OMV signal and minimize debris signals, we utilized a minimal threshold on red fluorescence to capture signal from DiI-labeled OMVs. An assay mixture containing 0.05 µg/ml OMVs (as protein) in 10 mM HEPES (pH 7.4), 50 mM NaCl, and glutathione *S*-transferase 75 µg/ml (carrier protein to prevent adsorption) was prepared for each size of F-dex at each Bax concentration, and samples were transferred to a 96-well plate. Each row on the 96-well plate corresponded to OMVs loaded with a different-sized F-dex and permeabilized with a specified Bax concentration, and each column corresponded to a 5-min time point. Time points for the assay were collected in this manner to reduce excessive sample agitation, which caused the OMV population to decrease, possibly reflecting adsorption to the wells or mechanical disruption. The use of a 96-well plate with premixed samples transferred into individual wells for each time point eliminated these issues. To aliquot and initialize sample analysis required 2–3 min of time, which

was accounted for when calculating the contributions from gradual and all-or-none release.

Our previous studies of dextran release in bulk populations of OMVs used an anti-fluorescein antibody to quench the fluorescence of released dextrans (Kushnareva *et al.*, 2012). However, this antibody could not be used here, because it can be assumed that the antibody, around the size of 70-kDa dextran (Supplemental Figure 5A), can enter into OMVs through the large Bax-induced pores, thus quenching large dextrans still entrapped there. We reasoned that a quenching antibody was unnecessary for our studies using flow cytometry because we could resolve the signals of fluorescent OMVs and free F-dex.

Numerical analyses

Histogram plots corresponding to F-dex fluorescence intensity versus event counts were generated with FlowJo 9.7.6 software for each assay condition at each time point. For each time point, the area (amplitude) and center (MFI) of the main OMV histogram peak was determined with Prism 6 software using a nonlinear curve fit to the sum of two log-Gaussian (log-normal) distributions. We fixed the first Gaussian peak (empty OMVs) to the MFI value of fully permeabilized OMVs, determined by incubating for 2 h a sample of each preparation of dextran-loaded OMVs with cBid and 20 nM Bax. The other Gaussian (partially full OMVs) was left unconstrained. Curve fitting was used to estimate the amplitude and width of the empty peak, as well as the amplitude, width, and center (MFI) of the partially full peak (see the text; Figure 5A).

Baseline values for the MFI of fully permeabilized vesicles were obtained for each preparation of F-dex–loaded OMVs from OMVs treated for 2 h with a high concentration (20 nM) of Bax to ensure near-complete dextran release. MFI values were normalized independently in each experiment for each preparation of F-dex–loaded OMVs, with 0% corresponding to the baseline sample and 100% corresponding to the fully loaded sample. Amplitudes were normalized to the fully loaded sample for each preparation of F-dex–loaded OMVs.

Consistent with previous studies, we typically observed a lag phase before the start of the permeabilization phase (Kushnareva *et al.*, 2012). However, because of the 2–3 min needed for sample handling, we were unable to measure the length of this early phase accurately. We fitted a simple exponential decay model in Prism to determine the kinetic rate constant (k) of the normalized MFI for the subsequent permeabilization phase. Rates were determined only for gradual release, as this mode of release was predominant over all-or-none release. As the number of intact OMVs was nearly constant, it follows that the rate of change of MFI is essentially proportional to the rate of F-dex release via the gradual mode (see the first term on the right side of Eq. 2).

Relative contributions of gradual and all-or-none modes of dextran release were calculated as follows: At time t, the total dextran content is the product of the number of vesicles and the fluorescence intensity:

$$C(t) = n(t) \times f(t) \quad (1)$$

where C is the total dextran content, n is the number of vesicles (corresponding to the peak amplitude), and f is the mean fluorescence intensity (peak center).

From the product rule of basic calculus, the rate of change of total dextran release can then be separated into two terms:

$$\frac{dC}{dt} = N(t) \times \frac{df}{dt} + f(t) \times \frac{dN}{dt} = G(t) + A(t) \quad (2)$$

where $G(t)$ is the rate of release via the gradual mode and $A(t)$ is the rate of release via the all-or-none mode. At time t, the cumulative contribution from the gradual release mode is then $\int_0^t G(t)\,dt$, and the cumulative contribution from the all-or-none release mode is $\int_0^t A(t)\,dt$.

For analysis of the discrete data sets generated by flow analysis, derivatives in these formulas were estimated as the slopes of line segments connecting data points, and the integrals were estimated by summing rectangles under the curves.

DLS

DLS was performed using a Zetasizer Nano-ZS (Malvern Instruments). The instrument was set to acquire three measurements, each consisting of 11–18 scans of the sample at 25°C. Results were copied from Zetasizer 6.20 software into Prism 6 software for analysis. The average of the three measurements is displayed for each sample. For determination of OMV size, 1 µl of OMVs at a protein concentration of ~0.5 mg/ml was added to 800 µl of 10 mM HEPES, 1 mM EDTA. For determination of 2000-kDa F-dex size, 10 µl of 5 mg/ml dextran was added to 800 µl of 10 nM NaCl. All buffers and solutions used for diluting samples for analysis by DLS were passed through a 100-nm filter before use.

Size-exclusion chromatography

Each FITC-dextran species was applied to a Superose 6 column (GE) and eluted with 10 mM HEPES (pH 7.4), 100 mM NaCl. Fractions were collected (0.9 ml), and elution of F-dex species in the fractions was detected by absorbance at 280 nm, which was confirmed by fluorescence spectroscopy (unpublished observations).

Cryo-EM

OMVs were isolated without dextran loading. The concentration of OMVs was adjusted to 0.5–0.8 mg/ml as protein, and they were incubated with Bax (812 nM or 3.25 µM) and cBid (420 nM or 2.5 µM) at 22°C for 20–90 min before freezing. Because the cryo-EM method requires a relatively high concentration of vesicles, we needed to use higher concentrations of Bax and cBid than those used for functional studies. Cryo-EM was performed as previously described (Baker *et al.*, 1999). Briefly, the vesicle suspensions were deposited to holey Quantifoil grids, blotted of excess fluid with Whatman filter paper for a few seconds, and immediately plunge-frozen in liquid ethane. The grids were inspected with a Tecnai G2 electron microscope (FEI) at 200 kV with ~10 µm underfocus at nominal magnifications of 5000× (low magnification) or 14,000–25,000× (high magnification). The vesicles were visualized with a CCD camera (Gatan). The OMVs were counted and categorized according to whether there was 1) no discontinuity in the membrane or 2) a gap/opening in the membrane. We also observed other kinds of membrane deformations, but they were present in both untreated and treated vesicles with the same frequency and were therefore considered artifacts, presumably arising from liquid flow during the freezing process. The pore size was estimated simply by a ruler-based measurement of the membrane gaps seen in micrographs. The actual distance (in nanometers) was calculated in reference to the scale bar in each image.

ACKNOWLEDGMENTS

Our use of the University of California–San Diego (UCSD) Cryo-Electron Microscopy Facility was supported by National Institutes of Health (NIH) grants to Timothy S. Baker and a gift from the Agouron Institute to UCSD. Technical assistance of Norm Olson (UCSD Cryo-EM Facility), Niema Razavian (La Jolla Institute), and Tatjana Orlic and

Giuseppe Destito (Kyowa Hakko Kirin California) is greatly appreciated. We thank Cheryl Kim (La Jolla Institute) for her helpful discussions and assistance with flow cytometry and Yulia Kushnareva and Alex Andreyev for helpful discussions and/or critical reading of the manuscript. This work was supported by NIH grants R01-GM062289 (to D.D.N.) and R01-GM086389 (to T.K.).

REFERENCES

Baker TS, Olson NH, Fuller SD (1999). Adding the third dimension to virus life cycles: three-dimensional reconstruction of icosahedral viruses from cryo-electron micrographs. Microbiol Mol Biol Rev 63, 862–922.

Basanez G, Sharpe JC, Galanis J, Brandt TB, Hardwick JM, Zimmerberg J (2002). Bax-type apoptotic proteins porate pure lipid bilayers through a mechanism sensitive to intrinsic monolayer curvature. J Biol Chem 277, 49360–49365.

Billen LP, Kokoski CL, Lovell JF, Leber B, Andrews DW (2008). Bcl-XL inhibits membrane permeabilization by competing with Bax. PLoS Biol 6, e147.

Bleicken S, Classen M, Padmavathi PV, Ishikawa T, Zeth K, Steinhoff HJ, Bordignon E (2010). Molecular details of Bax activation, oligomerization, and membrane insertion. J Biol Chem 285, 6636–6647.

Bleicken S, Landeta O, Landajuela A, Basanez G, Garcia-Saez AJ (2013). Proapoptotic Bax and Bak form stable protein-permeable pores of tunable size. J Biol Chem 288, 33241–33252.

Bohrer MP, Patterson GD, Carroll PJ (1984). Hindered diffusion of dextran and ficoll in microporous membranes. Macromolecules 17, 1170–1173.

Braun CR, Mintseris J, Gavathiotis E, Bird GH, Gygi SP, Walensky LD (2010). Photoreactive stapled BH3 peptides to dissect the BCL-2 family interactome. Chem Biol 17, 1325–1333.

Chen L, Willis SN, Wei A, Smith BJ, Fletcher JI, Hinds MG, Colman PM, Day CL, Adams JM, Huang DC (2005). Differential targeting of prosurvival Bcl-2 proteins by their BH3-only ligands allows complementary apoptotic function. Mol Cell 17, 393–403.

Chipuk JE, McStay GP, Bharti A, Kuwana T, Clarke CJ, Siskind LJ, Obeid LM, Green DR (2012). Sphingolipid metabolism cooperates with BAK and BAX to promote the mitochondrial pathway of apoptosis. Cell 148, 988–1000.

Chipuk JE, Moldoveanu T, Llambi F, Parsons MJ, Green DR (2010). The BCL-2 family reunion. Mol Cell 37, 299–310.

Czabotar PE, Westphal D, Dewson G, Ma S, Hockings C, Fairlie WD, Lee EF, Yao S, Robin AY, Smith BJ, *et al*. (2013). Bax crystal structures reveal how BH3 domains activate Bax and nucleate its oligomerization to induce apoptosis. Cell 152, 519–531.

Dejean LM, Martinez-Caballero S, Guo L, Hughes C, Teijido O, Ducret T, Ichas F, Korsmeyer SJ, Antonsson B, Jonas EA, Kinnally KW (2005). Oligomeric Bax is a component of the putative cytochrome c release channel MAC, mitochondrial apoptosis-induced channel. Mol Biol Cell 16, 2424–2432.

Dewson G, Kluck RM (2009). Mechanisms by which Bak and Bax permeabilise mitochondria during apoptosis. J Cell Sci 122, 2801–2808.

Dewson G, Kratina T, Sim HW, Puthalakath H, Adams JM, Colman PM, Kluck RM (2008). To trigger apoptosis, Bak exposes its BH3 domain and homodimerizes via BH3:groove interactions. Mol Cell 30, 369–380.

Eskes R, Antonsson B, Osen-Sand A, Montessuit S, Richter C, Sadoul R, Mazzei G, Nichols A, Martinou JC (1998). Bax-induced cytochrome C release from mitochondria is independent of the permeability transition pore but highly dependent on Mg^{2+} ions. J Cell Biol 143, 217–224.

Estaquier J, Arnoult D (2007). Inhibiting Drp1-mediated mitochondrial fission selectively prevents the release of cytochrome c during apoptosis. Cell Death Differ 14, 1086–1094.

Etxebarria A, Terrones O, Yamaguchi H, Landajuela A, Landeta O, Antonsson B, Wang HG, Basanez G (2009). Endophilin B1/Bif-1 stimulates BAX activation independently from its capacity to produce large scale membrane morphological rearrangements. J Biol Chem 284, 4200–4212.

Gavathiotis E, Suzuki M, Davis ML, Pitter K, Bird GH, Katz SG, Tu HC, Kim H, Cheng EH, Tjandra N, Walensky LD (2008). BAX activation is initiated at a novel interaction site. Nature 455, 1076–1081.

Granath KA (1958). Solution properties of branched dextrans. J Colloid Sci 13, 308–328.

Guihard G, Bellot G, Moreau C, Pradal G, Ferry N, Thomy R, Fichet P, Meflah K, Vallette FM (2004). The mitochondrial apoptosis-induced channel (MAC) corresponds to a late apoptotic event. J Biol Chem 279, 46542–46550.

Hanahan D, Weinberg RA (2011). Hallmarks of cancer: the next generation. Cell 144, 646–674.

Hilgendorf KI, Leshchiner ES, Nedelcu S, Maynard MA, Calo E, Ianari A, Walensky LD, Lees JA (2013). The retinoblastoma protein induces apoptosis directly at the mitochondria. Genes Dev 27, 1003–1015.

Kluck RM, Bossy-Wetzel E, Green DR, Newmeyer DD (1997). The release of cytochrome c from mitochondria: a primary site for Bcl-2 regulation of apoptosis. Science 275, 1132–1136.

Kluck RM, Esposti MD, Perkins G, Renken C, Kuwana T, Bossy-Wetzel E, Goldberg M, Allen T, Barber MJ, Green DR, Newmeyer DD (1999). The pro-apoptotic proteins, Bid and Bax, cause a limited permeabilization of the mitochondrial outer membrane that is enhanced by cytosol. J Cell Biol 147, 809–822.

Kushnareva Y, Andreyev AY, Kuwana T, Newmeyer DD (2012). Bax activation initiates the assembly of a multimeric catalyst that facilitates Bax pore formation in mitochondrial outer membranes. PLoS Biol 10, e1001394.

Kuwana T, Bouchier-Hayes L, Chipuk JE, Bonzon C, Sullivan BA, Green DR, Newmeyer DD (2005). BH3 domains of BH3-only proteins differentially regulate Bax-mediated mitochondrial membrane permeabilization both directly and indirectly. Mol Cell 17, 525–535.

Kuwana T, Mackey MR, Perkins G, Ellisman MH, Latterich M, Schneiter R, Green DR, Newmeyer DD (2002). Bid, Bax, and lipids cooperate to form supramolecular openings in the outer mitochondrial membrane. Cell 111, 331–342.

Landeta O, Landajuela A, Gil D, Taneva S, Di Primo C, Sot B, Valle M, Frolov VA, Basanez G (2011). Reconstitution of proapoptotic BAK function in liposomes reveals a dual role for mitochondrial lipids in the BAK-driven membrane permeabilization process. J Biol Chem 286, 8213–8230.

Lartigue L, Kushnareva Y, Seong Y, Lin H, Faustin B, Newmeyer DD (2009). Caspase-independent mitochondrial cell death results from loss of respiration, not cytotoxic protein release. Mol Biol Cell 20, 4871–4884.

Letai A, Bassik MC, Walensky LD, Sorcinelli MD, Weiler S, Korsmeyer SJ (2002). Distinct BH3 domains either sensitize or activate mitochondrial apoptosis, serving as prototype cancer therapeutics. Cancer Cell 2, 183–192.

Liu X, Kim CN, Yang J, Jemmerson R, Wang X (1996). Induction of apoptotic program in cell-free extracts: requirement for dATP and cytochrome c. Cell 86, 147–157.

Llambi F, Moldoveanu T, Tait SW, Bouchier-Hayes L, Temirov J, McCormick LL, Dillon CP, Green DR (2011). A unified model of mammalian BCL-2 protein family interactions at the mitochondria. Mol Cell 44, 517–531.

Lucken-Ardjomande S, Montessuit S, Martinou JC (2008). Contributions to Bax insertion and oligomerization of lipids of the mitochondrial outer membrane. Cell Death Differ 15, 929–937.

Martinez-Caballero S, Dejean LM, Kinnally MS, Oh KJ, Mannella CA, Kinnally KW (2009). Assembly of the mitochondrial apoptosis-induced channel, MAC. J Biol Chem 284, 12235–12245.

Moldoveanu T, Grace CR, Llambi F, Nourse A, Fitzgerald P, Gehring K, Kriwacki RW, Green DR (2013). BID-induced structural changes in BAK promote apoptosis. Nat Struct Mol Biol 20, 589–597.

Montessuit S, Somasekharan SP, Terrones O, Lucken-Ardjomande S, Herzig S, Schwarzenbacher R, Manstein DJ, Bossy-Wetzel E, Basanez G, Meda P, Martinou JC (2010). Membrane remodeling induced by the dynamin-related protein Drp1 stimulates Bax oligomerization. Cell 142, 889–901.

Muchmore SW, Sattler M, Liang H, Meadows RP, Harlan JE, Yoon HS, Nettesheim D, Chang BS, Thompson CB, Wong S-L, *et al*. (1996). X-ray and NMR structure of human Bcl-xL, an inhibitor of programmed cell death. Nature 381, 335–341.

Munoz-Pinedo C, Guio-Carrion A, Goldstein JC, Fitzgerald P, Newmeyer DD, Green DR (2006). Different mitochondrial intermembrane space proteins are released during apoptosis in a manner that is coordinately initiated but can vary in duration. Proc Natl Acad Sci USA 103, 11573–11578.

Schafer B, Quispe J, Choudhary V, Chipuk JE, Ajero TG, Du H, Schneiter R, Kuwana T (2009). Mitochondrial outer membrane proteins assist Bid in Bax-mediated lipidic pore formation. Mol Biol Cell 20, 2276–2285.

Takahashi Y, Karbowski M, Yamaguchi H, Kazi A, Wu J, Sebti SM, Youle RJ, Wang HG (2005). Loss of Bif-1 suppresses Bax/Bak conformational change and mitochondrial apoptosis. Mol Cell Biol 25, 9369–9382.

Tanaka A, Youle RJ (2008). A chemical inhibitor of DRP1 uncouples mitochondrial fission and apoptosis. Mol Cell 29, 409–410.
Terrones O, Antonsson B, Yamaguchi H, Wang HG, Liu J, Lee RM, Herrmann A, Basanez G (2004). Lipidic pore formation by the concerted action of proapoptotic BAX and tBID. J Biol Chem 279, 30081–30091.
Tilley SJ, Saibil HR (2006). The mechanism of pore formation by bacterial toxins. Curr Opin Struct Biol 16, 230–236.
van der Pol E, van Gemert MJ, Sturk A, Nieuwland R, van Leeuwen TG (2012). Single vs. swarm detection of microparticles and exosomes by flow cytometry. J Thromb Haemost 10, 919–930.
Van Loo G, Demol H, van Gurp M, Hoorelbeke B, Schotte P, Beyaert R, Zhivotovsky B, Gevaert K, Declercq W, Vandekerckhove J, Vandenabeele P (2002). A matrix-assisted laser desorption ionization post-source decay (MALDI-PSD) analysis of proteins released from isolated liver mitochondria treated with recombinant truncated Bid. Cell Death Differ 9, 301–308.
Volkmann N, Marassi FM, Newmeyer DD, Hanein D (2014). The rheostat in the membrane: BCL-2 family proteins and apoptosis. Cell Death Differ 21, 206–215.
Westphal D, Kluck RM, Dewson G (2014). Building blocks of the apoptotic pore: how Bax and Bak are activated and oligomerize during apoptosis. Cell Death Differ 21, 196–205.
Xu XP, Zhai D, Kim E, Swift M, Reed JC, Volkmann N, Hanein D (2013). Three-dimensional structure of Bax-mediated pores in membrane bilayers. Cell Death Dis 4, e683.
Yang J, Liu X, Bhalla K, Kim CN, Ibrado AM, Cai J, Peng T-I, Jones DP, Wang X (1997). Prevention of apoptosis by Bcl-2: release of cytochrome c from mitochondria blocked. Science 275, 1129–1132.